JOURNAL OF AIRCRAFT
Vol. 36, No. 2, March–April 1999

Vortex Characteristics of Pitching Double-Delta Wings

Lars E. Ericsson*
Mountain View, California 94040

The increasing performance demands on advanced aircraft, including maneuvers at high angles of attack, has led to a need for the prediction of vehicle aerodynamics that are dominated by separated flow effects. For aircraft with highly swept wing leading edges, the challenge is to fully understand the flow physics behind the observed dramatic effects of vortex breakdown. An analysis has been performed to define the physical flow processes that could have generated the highly unusual rolling-moment characteristics measured on a 76-deg/40-deg double-delta wing, describing high-amplitude pitch oscillations at high angles of attack and nonzero angle of sideslip.

Nomenclature

b = wingspan
c = wing root chord
f = oscillation frequency
k = reduced frequency, $\omega c/2U_\infty$
l = rolling moment, coefficient $C_l = l/(\rho_\infty U_\infty^2/2)Sb$
p = static pressure, coefficient $C_p = (p - p_\infty)/(\rho_\infty U_\infty^2/2)$
S = reference area, projected wing area
s = local semispan
U = horizontal velocity
x = chordwise coordinate
y = spanwise coordinate
α = angle of attack
β = angle of sideslip
Δ = increment
η = dimensionless y coordinate, y/s
Λ = leading-edge sweep
ξ = dimensionless x coordinate, x/c
ρ = air density
σ = inclination of roll axis
ϕ = roll angle
ω = angular frequency, $2\pi f$

Subscripts

B = breakdown
C = camber
0 = time-average value
∞ = freestream conditions

Differential symbol

$\dot{\alpha}$ = $\partial\alpha/\partial t$

Introduction

At moderate angles of attack, the vortices from the forward-inner and aft-outer delta wing leading edges of a double-delta wing each generate their individual loads, as demonstrated by the experimental results[1] in Fig. 1. At high angles of attack, the two vortices start to interact with each other. Although the interaction in general involves a starting phase in which the two vortices spiral around each other in a helical mode, the development with a further increase of the angle of attack is very different, depending on the relative magnitudes of the leading-edge sweeps of the two delta wings. In the case of a true double-delta wing, both wings would support leading-edge vortices by themselves, in the absence of the other wing, whereas in the case of the straked wing, the outer wing will have a leading-edge vortex only in the presence of the inner, highly swept delta wing: the strake. An example of the former is the 77.2-deg/59-deg double-delta,[2] shown in Fig. 2, where the two vortices spiral around each other while keeping their identity. The result is an increase and redistribution of the loading generated by the outer delta wing alone[3] (Fig. 3).

An example of the straked-wing geometry is the one investigated by Cunningham and den Boer[4] (Fig. 4). In this case, the interaction leads to the breakdown of both vortices (Fig. 5), starting with the outer wing vortex according to the experimental results[4,5] in Fig. 6, showing the $C_p(\eta)$ distribution in section 2. The experimental results in Fig. 5 show that at $\alpha = 19$ deg, two individual vortices exist at section 2, whereas the vortices have merged before section 3. When α is increased to 22.4 deg, the pressure distribution in sections 2 and 3 remain relatively unchanged, indicating that the flow sketch in Fig. 5 for $\alpha = 22.4$ deg should be very similar to that for $\alpha = 19$ deg. That is, vortex breakdown has not advanced to section 2 until $\alpha > 22.4$ deg. The flow sketch for $\alpha = 22.4$ deg fits better to the $C_p(\eta)$ distribution for $\alpha = 36$ deg, showing merger of the vortices at section 2 and breakdown of the merged vortices occurring at section 3. At $\alpha = 42.3$ deg, the pressure distribution is flat in both sections, having roughly the same plateau pressure, indicating that breakdown of both vortices occurs forward of section 2. That is, $C_p(\eta)$ shows that the flow picture for $\alpha = 42.3$ deg should be the one to use for $\alpha = 36$ deg. That is, instead of increasing the outer wing loading (Fig. 3), the interaction causes a decrease through the incurred vortex breakdown (Fig. 5).

To appreciate the fundamental difference in flow physics between double-delta and straked-wing geometries, one needs to take a closer look at the basic aerodynamics of the two wing configurations. Whereas, in the former case, the outer delta wing by itself would generate a leading-edge vortex above a certain angle of attack, the value of which depends on the leading-edge cross-sectional geometry,[6] in the latter case, only a partial leading-edge vortex would exist. As this has been observed even when the wing has a 49.4-deg leading-edge sweep[7] (Fig. 7), it certainly would be the case for the 40-deg sweep in Fig. 4. Thus, the outer wing leading-edge vortex in Fig. 4 exists only in the presence of the flow induced by the strake vortex. In view of these flow physics considerations, one must expect that the vortex interaction would be very sensitive to sideslip, a problem addressed in Ref. 4.

Presented as Paper 97-3574 at the AIAA Atmospheric Flight Mechanics Conference, New Orleans, LA, Aug. 11–13, 1997; received Oct. 8, 1997; revision received Oct. 8, 1998; accepted for publication Oct. 9, 1998.

*Engineering Consultant. Fellow AIAA.

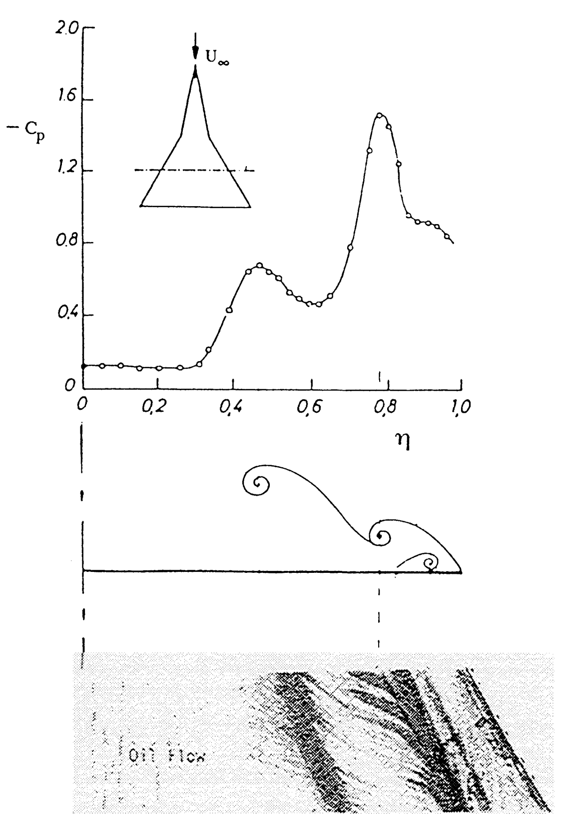

Fig. 1 Individual vortex-induced loads on a 72-deg/59-deg double-delta wing.[1]

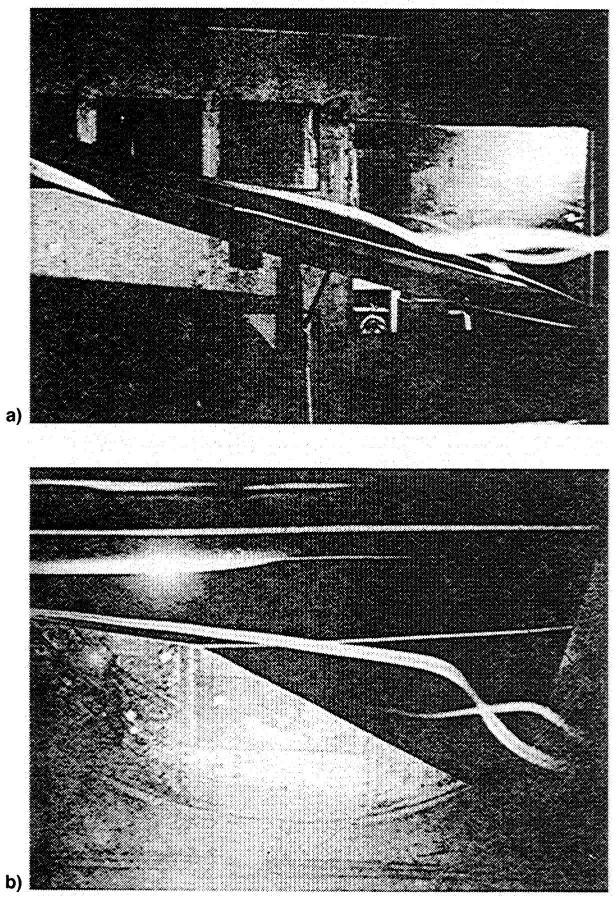

Fig. 2 Interacting leading-edge vortices on a double-delta wing[2]: a) side and b) plan views.

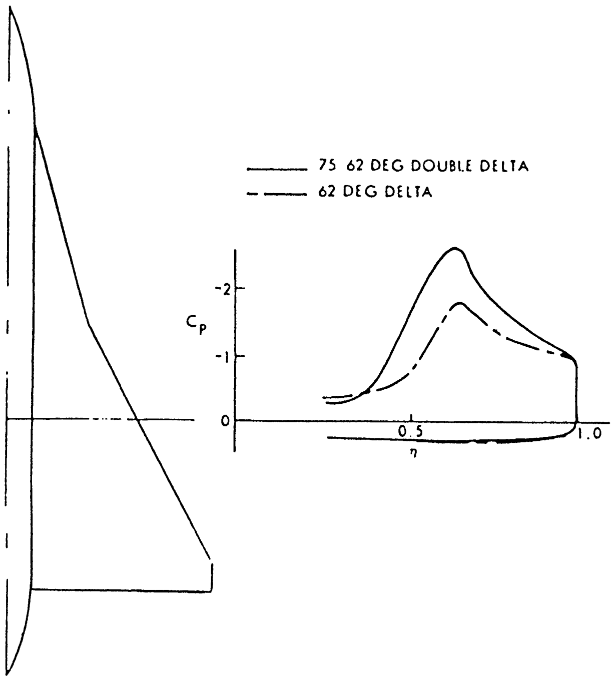

Fig. 3 Effect of 75-deg inner delta wing on the loads of a 62-deg delta wing.[3]

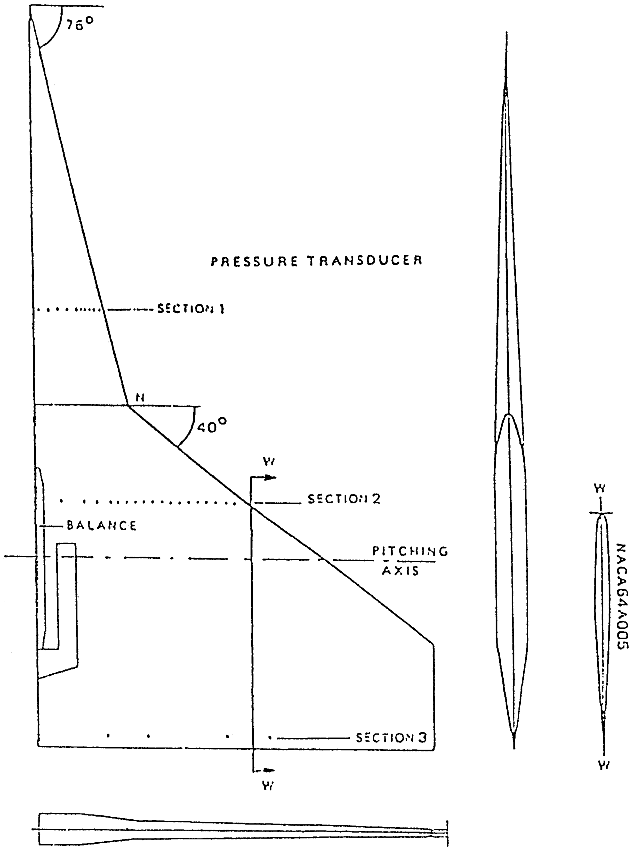

Fig. 4 76-deg/40-deg straked wing geometry.[4]

Discussion

Figure 8 shows how an angle of sideslip of $\beta = -5$ deg dramatically changes the $C_l(\alpha)$ characteristics at $\alpha > 18$ deg of the tested straked wing geometry (Fig. 4). The sideslip is likely to have a profound effect on the vortex interaction, and one can expect that the sideslip will produce critical flow states similar to those generated at $|\phi| \approx 5$ and 9 deg in the case of

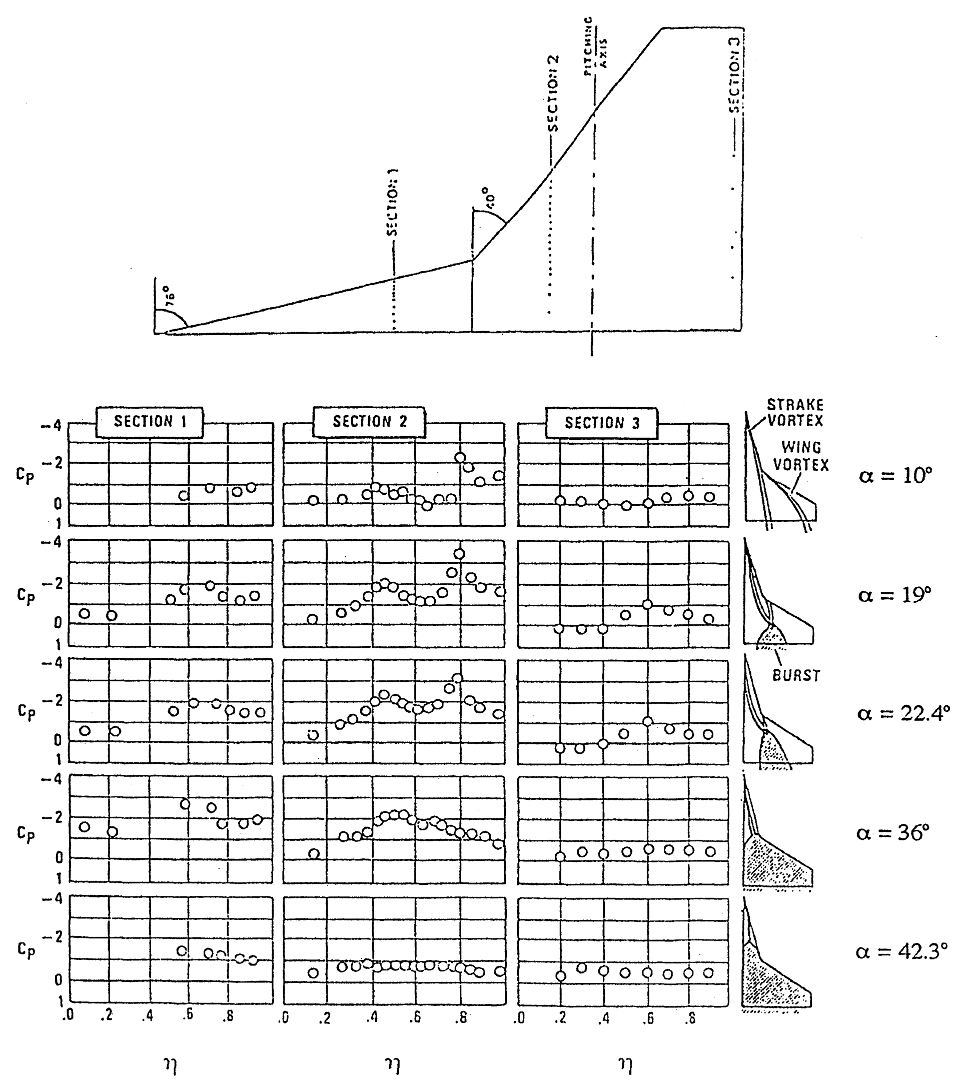

Fig. 5 Load distribution and vortex geometries at various angles of attack on 76-deg/40-deg straked wing geometry.[4,5]

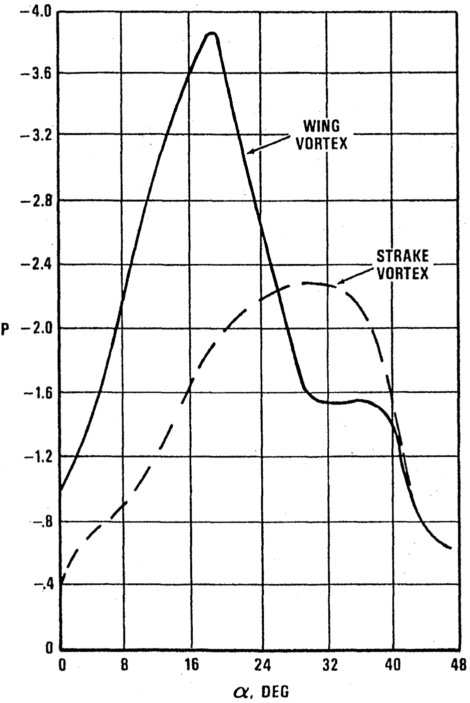

Fig. 6 Suction pressures under wing and strake vortices.[4,5]

a 65-deg delta-wing-body configuration[8–10] (Fig. 9). In both cases, it is the breakdown movement on windward and leeward wing halves that generate the highly nonlinear, almost discontinuous $C_l(\alpha)$ characteristics. In both cases, the breakdown movement is dictated by the effective leading-edge sweep Λ_{eff}:

$$\Lambda_{\mathrm{eff}} = \Lambda \pm \Delta\Lambda \tag{1}$$

$$\Delta\Lambda = \tan^{-1}(\tan \sigma \cos \phi) \tag{1a}$$

$$\Delta\Lambda = \tan^{-1}(\tan \beta \sec \alpha) \tag{1b}$$

The plus–minus sign in Eq. (1) refers to the leeward and windward wing halves, respectively. In both cases, Figs. 8 and 9, the incurred increase of the leading-edge sweep on the leeward wing half delays vortex breakdown, and the decrease of the sweep on the windward wing half promotes the breakdown. Two critical flow states exist for the straked wing, as was also the case for the 65-deg delta wing in Fig. 9. In the present case, the critical states occur for zero sideslip at $\alpha \approx$ 18 and 36 deg, according to Fig. 8. Figure 5 shows that the former critical state consists of a change from two individual leading-edge vortices to the interactive, spiraling vortex configuration that results in breakdown of the wing vortex (Figs. 5 and 6). The critical state at $\alpha \approx$ 36 deg occurs when the vortex breakdown has reached the apex of the outer, main wing, the strake–wing juncture. A further increase of the angle of attack has little effect on the breakdown extent. Of course,

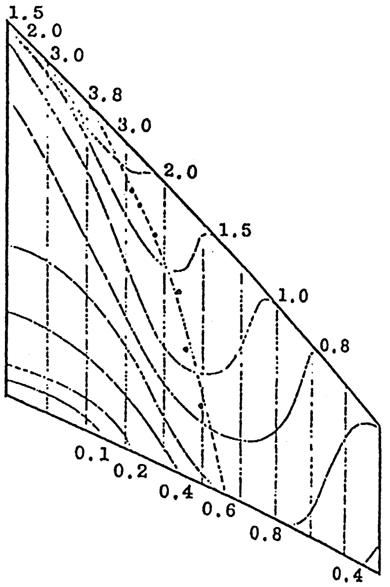

Fig. 7 Isobars at α = 20 deg on a 49.4-deg cropped arrowhead wing.[7]

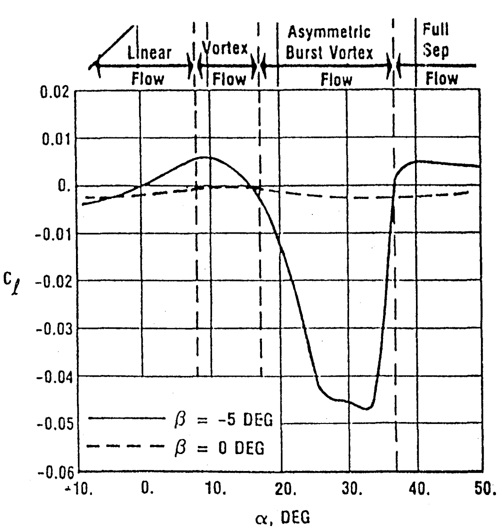

Fig. 8 Effect of sideslip on $C_l(\alpha)$ for the 76-deg/40-deg straked wing.[4]

at nonzero sideslip, the two critical states occur at different angles of attack for leeward and windward wing halves.

In Fig. 10 flow sketches are used as in Fig. 9 to illustrate the effect on the rolling moment at $\beta = -5$ deg of the two critical flow states at $\alpha \approx 18$ and 36 deg (Fig. 8). The data trend at $\alpha < 18$ deg is the one expected for unburst strake vortices, equivalent to the statically stabilizing $C_l(\phi)$ trend for a rolling slender wing in the absence of vortex breakdown.[11] At $\alpha > 18$ deg, the windward wing half at $\beta = -5$ deg experiences vortex breakdown that advances rapidly with increasing angle of attack until $\alpha \approx 25$ deg, where its advance is slowed down considerably, causing $C_l(\alpha)$ to bottom out. At $\alpha > 33$ deg, vortex breakdown starts occurring on the leeward wing half, advancing with increasing alpha until $\alpha \approx 36$ deg, where its extension becomes almost as large as for the windward wing half; i.e., both wing halves are completely stalled.

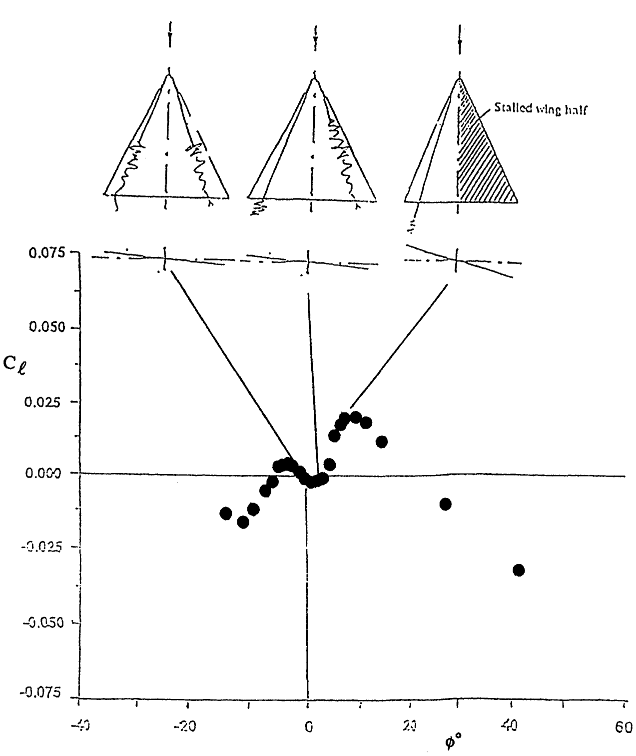

Fig. 9 Evolution of $C_l(\phi)$ characteristics for a 65-deg delta wing at σ = 30 deg.[10]

Unsteady Aerodynamic Characteristics

In view of the well-known large effects of pitch rate on delta wing vortex breakdown,[12] the $C_l(\alpha)$ characteristics in Fig. 10 for $\beta = -5$ deg should change dramatically for nonzero pitch rates. With $\alpha = 18$ deg being one of the critical states, one expects pitch oscillations into the region $\alpha > 18$ deg to show large rate-induced effects on the $C_l(\alpha)$ characteristics, based upon the large effects of roll rate observed for oscillations into a similar critical flow region for a 65-deg delta wing.[8-10] Figures 11–13 show the measured $C_l(\alpha)$ for 14-deg amplitude oscillations in pitch around α_0 = 10, 22, and 36 deg, respectively. Figure 11 shows significant effects of pitch rate on the $C_l(\alpha)$ loops, with upstroke and downstroke branches located asymmetrically relative to the steady (k = 0) $C_l(\alpha)$ characteristics. This asymmetry has also been observed for pure delta wings.[13-16] The asymmetry is caused by pitch-rate-induced camber effects on vortex breakdown,[12,17] as influenced by initial conditions through time-history effects.[18] The negative pitch-rate-induced camber on the downstroke can promote vortex breakdown much more than what the rate-induced positive camber on the upstroke can delay vortex breakdown, a fact well illustrated by the results in Fig. 11. Figures 12 and 13 show that the $C_l(\alpha)$ loops become more complex when the critical alpha range is penetrated further. It is apparent from Figs. 8 and 10 that in the range, 18 deg < α < 36 deg, the vortex breakdown occurring on one or both wing halves has a dominating effect on the $C_l(\alpha)$ characteristics. This fact will be exploited in the analysis of the experimental results in Figs. 11–13.

The pitch-rate-induced camber effect[12] (Fig. 14) will delay vortex breakdown during the upstroke and promote it during the downstroke. The experimental results for an 80-deg delta wing[17] (Fig. 15) demonstrate that the camber effect is much larger for $\Delta\alpha_c < 0$ (Fig. 15b) than for $\Delta\alpha_c > 0$ (Fig. 15a). Applying the information in Figs. 14 and 15 to Figs. 8 and 10, one concludes that for 18 deg < α < 25 deg, vortex breakdown will only occur on the left, windward wing half, where the pitch-rate-induced camber will delay vortex breakdown during the upstroke and promote it during the downstroke. At 25 deg $\leq \alpha \leq$ 36 deg, the pitch-rate-induced camber will decide which wing half dominates. Determining the pitch-rate-induced effect on the rolling moment in this α range is complicated by the fact that an increase of C_l cannot only be the result of the rate-induced delay of breakdown on the left, windward wing half, but can also be the result of the rate-induced promotion of breakdown on the right, leeward wing half, as

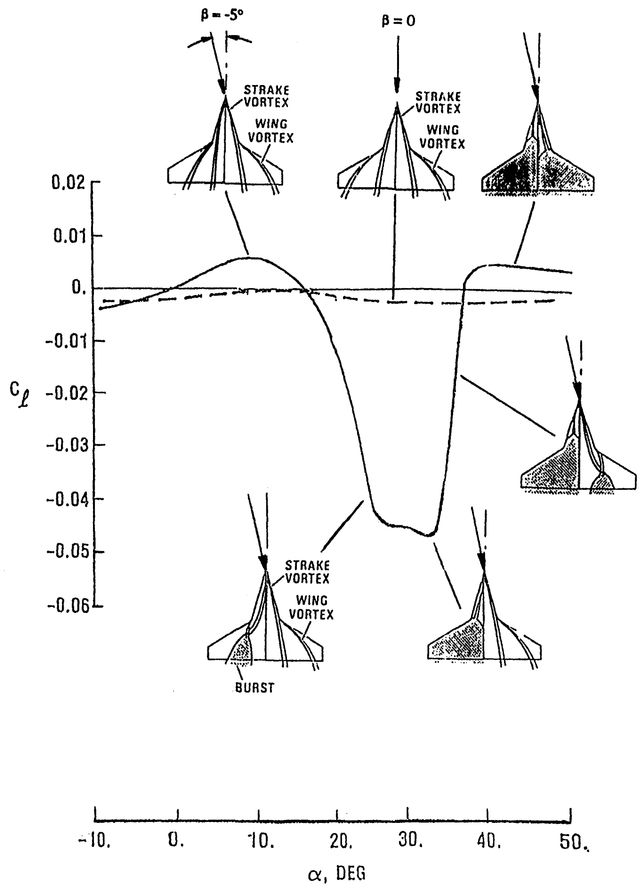

Fig. 10 Conceptual flow pictures illustrating the measured $C_l(\alpha)$ at β = −5 deg of the 76-deg/40-deg straked wing.

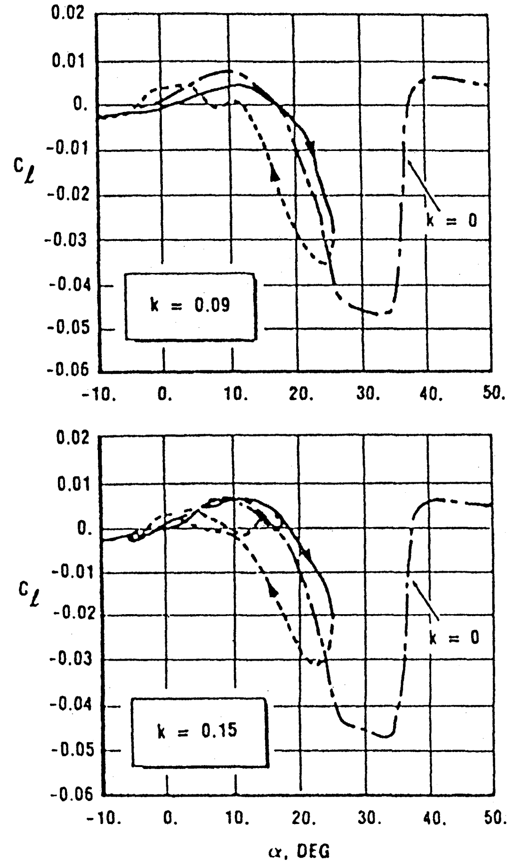

Fig. 11 Measured $C_l(\alpha)$ at β = −5 deg for 14-deg amplitude pitch oscillations around α_0 = 10 deg at k = 0.09 and 0.15.[4]

the delay of vortex breakdown will generate more lift and the promotion of breakdown less lift on the wing half where it occurs.

Thus, in the case of the unsteady $C_l(\alpha)$ characteristics in Fig. 11 for $-4 \text{ deg} \leq \alpha \leq 24$ deg, vortex breakdown will only occur on the left, windward wing half (Figs. 8 and 10). The reversal of the $C_l(\alpha)$ loops for $\alpha < 5$ deg, caused by vorticity lag effects,[19] will not be discussed. Here, the focus will be on the $C_l(\alpha)$ loops at high angles of attack, where vortex breakdown has a dominant effect. As can be deduced from Figs. 14 and 15, the positive, pitch-rate-induced camber generated during the upstroke will delay breakdown, whereas the effect of the negative camber generated during the downstroke will be the opposite. As was discussed earlier in connection with Figs. 14 and 15, the negative camber effect is of considerably larger magnitude than the positive camber effect, explaining the character of the high-alpha parts of the $C_l(\alpha)$ loops in Fig. 11. As expected, increasing the reduced frequency from k = 0.09 to 0.15, increased the displacement of the $C_l(\alpha)$ loops relative to the static characteristics.

As the dominating effect of vortex breakdown is only present on the left, windward wing half for $\alpha \leq 24$ deg (Figs. 8 and 10), the pitch-rate-induced effects on the dynamic $C_l(\alpha)$ loop branches in Figs. 11 and 12 are similar in nature for $\alpha <$ 24 deg. The upstroke branches in this α range show the expected dynamically equivalent steady (DES) characteristics.[18] The DES characteristics for a pitching delta wing are those measured in a static test with the cambered delta-wing geometry shown in Fig. 14c. The same characteristics can also be obtained by integrating the quasisteady load distribution generated by the pitch-rate-induced velocity distribution shown in Fig. 14b. The advantage with the DES characteristics is that they can be obtained in static tests with a suitably shaped model, as illustrated in Fig. 14 for a pitching delta wing, and in Fig. 16 for a rolling 65-deg delta wing. In the latter case, the DES characteristics were obtained in static tests with a thin sheet-metal model deformed as shown in the bottom sketch in the inset of Fig. 16. The predicted roll-rate-induced camber effect on the vortex breakdown[20] was verified by static tests with the DES model[19] (Fig. 16). The static results showed that the roll-rate-induced camber caused a shift $\Delta\xi_B \approx \pm 0.1$ at α = 30 deg.

As expected, for $\alpha < 24$ deg in Fig. 12, the pitch-rate-induced camber effect for k = 0.15 caused larger overshoot and undershoot of the static characteristics than k = 0.09. More remarkable is the large nonlinear effect of k during the downstroke for $24 \text{ deg} \leq \alpha \leq 36$ deg. This is the alpha region, discussed earlier, where vortex breakdown occurs on both wing halves. Going back to Fig. 10, at the left end of the bucket, one expects positive camber effects on the left, windward wing half to delay vortex breakdown and produce the measured rate-induced increase of $C_l(\alpha)$ during the upstroke. When considering the time-lag effects discussed later [Eqs. (3–8)], one expects this rate-induced camber effect to be present throughout the upstroke branch of the $C_l(\alpha)$ loop. At the opposite end, $\alpha > 30$ deg in Fig. 10, the left wing half is completely stalled, leaving it to the right, leeward wing half to produce the measured increase above static $C_l(\alpha)$ through the loss of lift caused by the rate-induced promotion of vortex breakdown. Note that the positive rate-induced camber effect can delay breakdown to exhibit at $\alpha >$ 25 deg, the geometry shown for static conditions at $\alpha < 25$ deg in Fig. 10; conversely, the negative rate-induced camber effect generates at $\alpha < 33$ deg, the static breakdown geometry shown at $\alpha > 33$ deg in Fig. 10.

Figure 12 shows that for k = 0.09 and 0.15, the upstroke $C_l(\alpha)$ characteristics were produced by the positive rate-induced camber on the left, windward wing half, increasing its lift, thereby generating the measured increase $\Delta C_l > 0$ above the static $C_l(\alpha)$ characteristics; and, as was the case in Fig. 11,

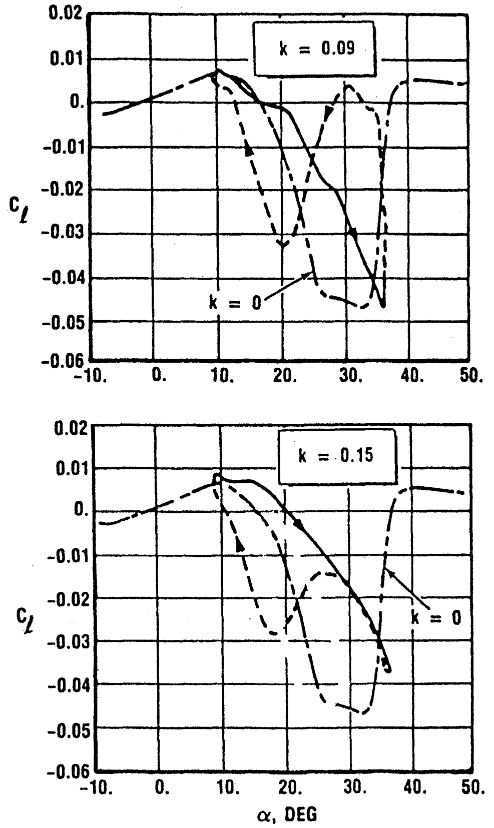

Fig. 12 Measured $C_l(\alpha)$ at $\beta = -5$ deg for 14-deg amplitude pitch oscillations around $\alpha_0 = 22$ deg at $k = 0.09$ and 0.15.[4]

ΔC_l is larger for $k = 0.15$ than for $k = 0.09$. Apparently, the pitch-rate-induced positive camber effect lasted to the end of the upstroke, $\alpha = 36$ deg. Judging by the shape of the upstroke branch of the $C_l(\alpha)$ curve, the right wing half never experienced the vortex breakdown responsible for the C_l bucket in Fig. 10. One possible explanation is that time-history effects caused the rate-induced positive camber effect to be present to the end of the upstroke.

The oscillatory change of angle of attack in Fig. 12 was

$$\alpha(t) = \alpha_0 + \Delta\alpha \sin \omega t \tag{2}$$

where $\alpha_0 = 22$ deg, and $\Delta\alpha = 14$ deg.

As a result of the time-history effect, which for the tested low frequencies can be approximated by the effect of a constant time lag Δt, the rate-induced camber existing at the end of the upstroke was generated at the angle of attack:

$$\alpha(t - \Delta t) = \alpha_0 + \Delta\alpha \sin(\pi/2 - \omega\Delta t) = \alpha_0 + \Delta\alpha \cos \omega\Delta t \tag{3}$$

The rate-induced camber existing at the end of the upstroke is roughly proportional to

$$\dot{\alpha}(t - \Delta t) = \Delta\alpha\omega \cos(\pi/2 - \omega\Delta t) = \Delta\alpha\omega \sin \omega\Delta t \tag{4}$$

With $\bar{U} \approx 0.70U_\infty$ being the convection velocity for pitch-rate-induced camber effects,[12] one obtains

$$\Delta t = c_0\xi_B/0.70U_\infty \tag{5}$$

$$\omega\Delta t = 2k\xi_B/0.70U_\infty \tag{6}$$

Combining Eqs. (4) and (6) gives

$$\dot{\alpha}(t - \Delta t)/\Delta\alpha\omega = 0.25 \text{ for } k = 0.09 \tag{7a}$$

$$\dot{\alpha}(t - \Delta t)/\Delta\alpha\omega = 0.41 \text{ for } k = 0.15 \tag{7b}$$

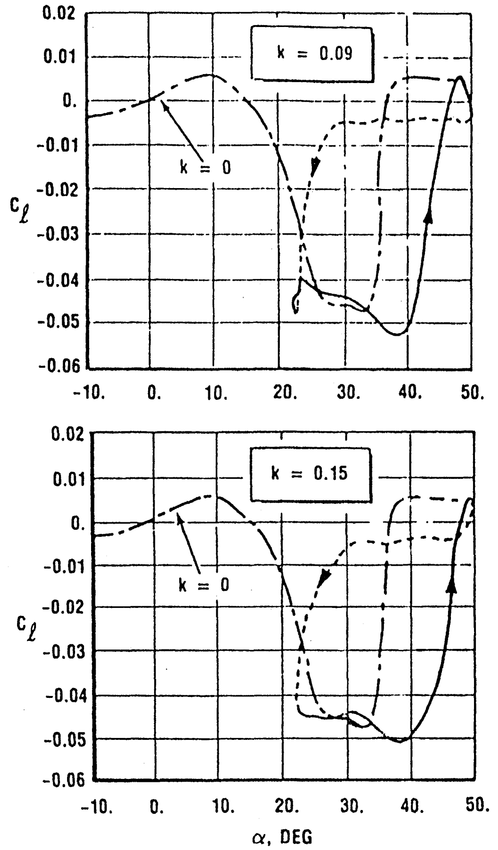

Fig. 13 Measured $C_l(\alpha)$ at $\beta = -5$ deg for 14-deg amplitude pitch oscillations around $\alpha_0 = 36$ deg at $k = 0.09$ and 0.15.[4]

That is,

$$\dot{\alpha}(t - \Delta t)_{k=0.15}/\dot{\alpha}(t - \Delta t)_{k=0.09} = 2.75 \tag{8}$$

Thus, the rate-induced positive camber existing at the end of the upstroke is significantly larger for $k = 0.15$ than for $k = 0.09$ in Fig. 12. Apparently, there exists some threshold value of the residual camber effect that has to be exceeded at the start of the downstroke before the dynamic $C_l(\alpha)$ characteristics exhibited for $k = 0.15$ will result. Tests with a similar straked-wing geometry[21] gave the results shown in Fig. 17. At $\alpha < 15$ deg, no vortex breakdown occurs on the model and the regular sideslip effect[6] generated a positive rolling moment at $\beta = -10$ deg. At this angle of sideslip, breakdown occurs early on the upwind wing half and will be extensive at $\alpha > 20$ deg, resulting in a completely stalled windward wing half at $\alpha = 30$ deg, where the leeward wing half has not yet started to experience vortex breakdown. This produces the minimum C_l value at $\alpha = 30$ deg. The leeside wing half becoming completely stalled at or before the value $\alpha = 39$ deg, measured at $\beta = 0$, may be the result of the body-shadow effect. When the angle of attack is increased to $\alpha \geq 35$ deg, the vortex breakdown moves to the apex also on the leeside wing half. As a result, the lift that was generated on that wing half upstream and downstream of a spiral vortex breakdown[22] is wiped out, completely eliminating the associated negative contribution to the rolling moment. The α hysteresis is of the usual type, showing the re-establishment of unburst vortices to occur at an angle of attack well below that causing the initial breakdown for increasing α. Once total stall has been established at $\alpha > 35$ deg, vortex breakdown configurations established at 20 deg $< \alpha <$ 33 deg for increasing α cannot be established for decreasing α.

Revisiting Fig. 12, one notices that for $k = 0.09$, the bottom value of the static $C_l(\alpha)$ characteristics was reached at the end

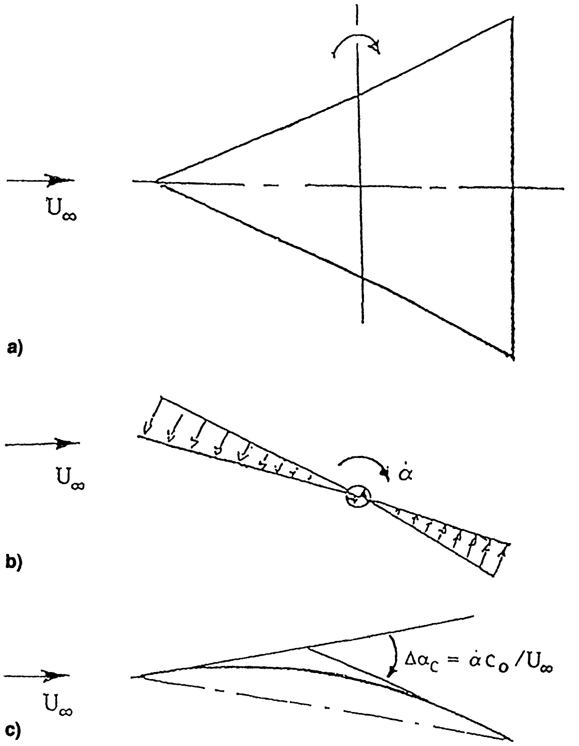

Fig. 14 Pitch-rate-induced camber effect.[12]

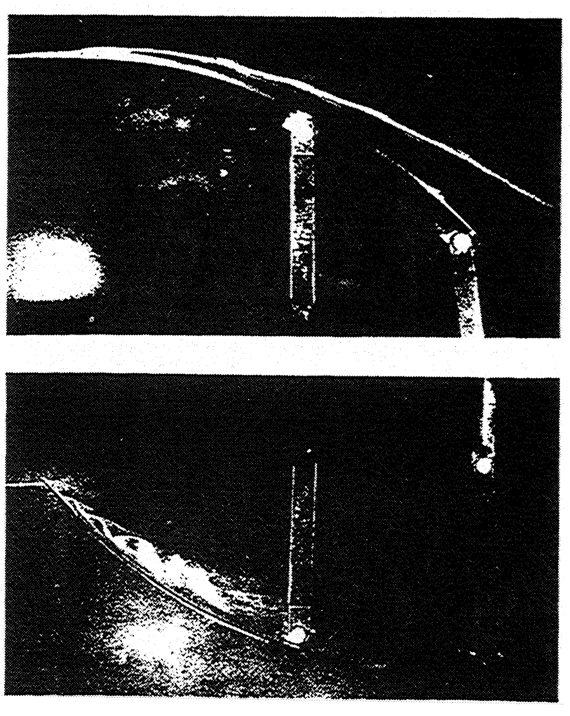

Fig. 15 Effect of static camber on the vortex breakdown on an 80-deg delta wing[17]: Local incidence a) increasing and b) decreasing with distance from apex.

of the upstroke. It appears, therefore, that in this case, the residual camber effect from the upstroke was below the threshold value at the beginning of the downstroke needed to overcome the static separation hysteresis illustrated by the $C_l(\alpha)$ characteristics in Fig. 17. Consequently, the deep-stall C_l level exists for a significant portion of the downstroke. In contrast, for the $k = 0.15$ case, the residual effect of the positive camber generated during the upstroke was large enough to prevent breakdown to reach the static conditions at the end of the upstroke, thereby preventing the downstroke branch of the α loop to realize the static hysteresis effect of vortex breakdown on the right, leeward wing half.

In Fig. 13, the pitch oscillations occur in the range, 22 deg $< \alpha <$ 50 deg, and the rate-induced camber effects on vortex breakdown are limited to the right, leeward wing half. During the upstroke, the positive rate-induced camber delays the occurrence of vortex breakdown, moving the dynamic $C_l(\alpha)$ loop an angle $\Delta\alpha > 0$ to the right of the static $C_l(\alpha)$ characteristics for increasing angle of attack, with $\Delta\alpha$ increasing with increasing k. For $k = 0.09$ and 0.15, the upstroke branch of the $C_l(\alpha)$

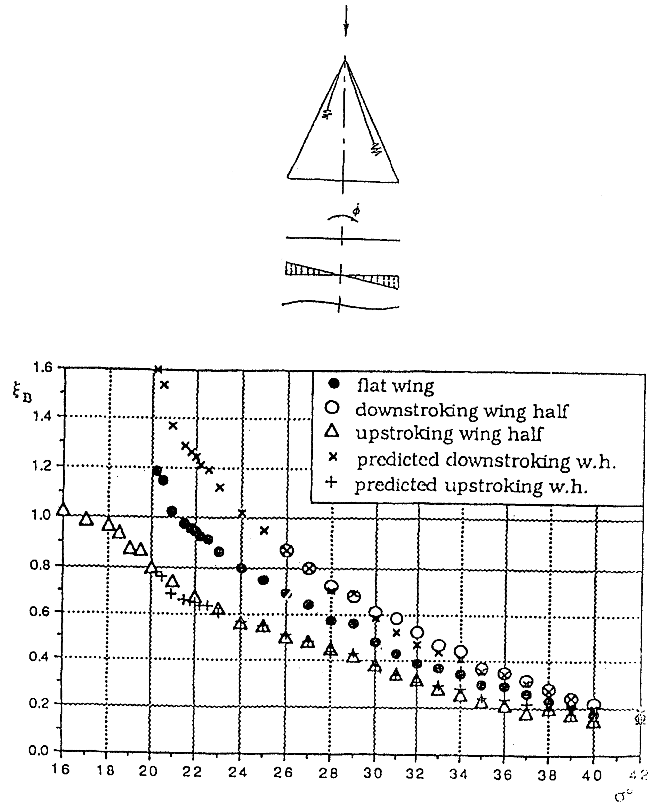

Fig. 16 Vortex breakdown location on deformed sheet-metal model of a 65-deg delta wing simulating the roll-rate-induced camber at $k\Delta\phi = 0.012$.[20]

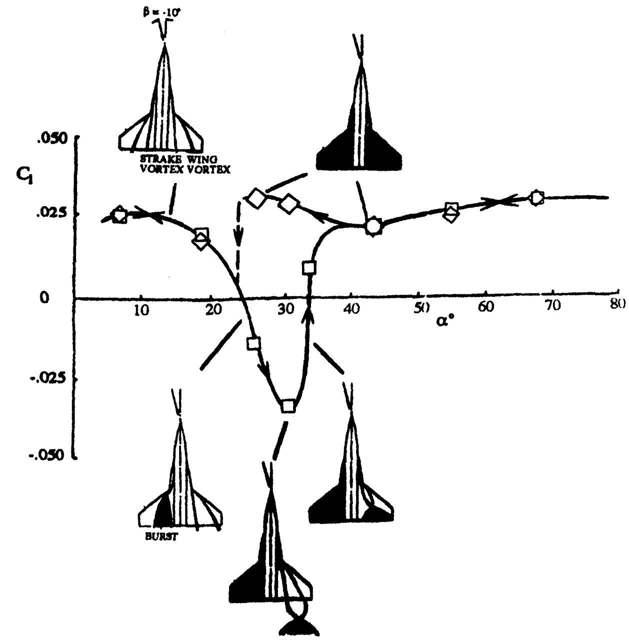

Fig. 17 Conceptual vortex characteristics for the measured $C_l(\alpha)$ at $\beta = -10$ deg on a generic combat aircraft model.[21]

loops reaches the static C_l level existing for completely stalled wing halves, well before the end of the upstroke in both cases. The negative pitch-rate-induced camber during the downstroke promotes breakdown, moving this branch of the $C_l(\alpha)$ loop an angle $\Delta\alpha > 0$ to the left of the static $C_l(\alpha)$ characteristics. The time-history effects are insignificant in this α region, and the dynamic $C_l(\alpha)$ loops are essentially determined by the DES aerodynamics. The experimental results in Figs. 10–13 indicate that control/vehicle dynamics coupling effects in high-alpha maneuvers may be of similar concern for double-deltas as for slender-nosed aircraft.[23]

Conclusions

An exploratory analysis of the experimental results obtained in pitch oscillation tests of a double-delta wing of the straked-wing category has shown that the lateral aerodynamics are at high angles of attack, dominated by the interaction between strake and wing vortices and the associated vortex breakdowns. This interaction is highly sensitive to pitch-rate-induced camber effects, and generates rolling-moment characteristics that exhibit highly nonlinear effects of pitch frequency and amplitude. This presents a challenge to the designer of advanced aircraft, who needs to predict the unsteady aerodynamics associated with high-alpha combat maneuvers.

References

[1] Krogmann, P., "Experimentelle und theoretische Untersuchungen an Doppeldelta Flügeln," *Aerodynamische Versuchsanstalt*, Bericht 68A35, Göttingen, Germany, July 1968.

[2] Sachs, A. H., Lundberg, R. E., and Hanson, C. W., "A Theoretical Investigation of the Aerodynamics of Slender Wing-Body Combinations Exibiting Leading-Edge Separation," NASA CR-719, March 1967.

[3] Wentz, W. H., Jr., and McMahon, M. C., "An Experimental Investigation of the Flow Fields About Delta and Double-Delta Wings at Low Speeds," NASA CR-521, Aug. 1966.

[4] Cunningham, A. M., Jr., and den Boer, R. G., "Steady and Unsteady Aerodynamics of a Pitching Straked Wing Model at High Angles of Attack," AGARD, CP-494, Oct. 1990 (Paper 29).

[5] Cunningham, A. M., Jr., and den Boer, R. G., Low-Speed Unsteady Aerodynamics of a Pitching Straked Wing at High Incidence—Part II: Harmonic Analysis," *Journal of Aircraft*, Vol. 30, No. 5, 1993, pp. 793–795.

[6] Ericsson, L. E., and King, H. H. C., Effect of Leading-Edge Cross-Sectional Geometry on Slender Wing Unsteady Aerodynamics," *Journal of Aircraft*, Vol. 30, No. 5, 1993, pp. 793–795.

[7] Garner, H. C., and Bryer, D. W., "Experimental Study of Surface Flow and Part-Span Vortex Layers on a Cropped Arrowhead Wing," Aerodynamic Research Council, R&M 3107, April 1957.

[8] Jobe, C. E., Hsia, A. H., Jenkins, J. E., and Addington, G. A., "Critical States and Flow Structure on a 65-Degree Delta Wing Oscillating in Roll," *Journal of Aircraft*, Vol. 33, No. 2, 1996, pp. 347–352.

[9] Ericsson, L. E., "Flow Physics of Critical States for Rolling Delta Wings," *Journal of Aircraft*, Vol. 32, No. 3, 1995, pp. 603–610.

[10] Ericsson, L. E., "Effect of Angle of Attack on Roll Characteristics of 65 Degree-Delta Wing," *Journal of Aircraft*, Vol. 34, No. 4, 1997, pp. 573–575.

[11] Ericsson, L. E., and King, H. H. C., "Rapid Prediction of Slender-Wing-Aircraft Stability Characteristics," *Journal of Aircraft*, Vol. 28, No. 3, 1991, pp. 354–356.

[12] Ericsson, L. E., "Pitch Rate Effects on Delta Wing Vortex Breakdown," *Journal of Aircraft*, Vol. 33, No. 3, 1996, pp. 639–642.

[13] Thompson, S. A., Bathill, S. M., and Nelson, R. C., "Separated Flow Field on a Slender Wing Undergoing Transient Pitching Motions," *Journal of Aircraft*, Vol. 28, No. 8, 1991, pp. 489–495.

[14] Guglieri, G., Onorato, M., and Quagliotti, F., "Breakdown Analysis on Delta Wing Vortices," *Zeitschrift Flugwissenshaft und Weltraumforschung*, Vol. 16, 1992, pp. 226–230.

[15] Atta, R., and Rockwell, D., "Hysteresis of Vortex Development and Breakdown on an Oscillating Delta Wing," *AIAA Journal*, Vol. 25, No. 11, 1987, pp. 1512, 1513.

[16] Atta, R., and Rockwell, D., "Leading-Edge Vortices Due to Low Reynolds Number Flow Past a Pitching Delta Wing," *AIAA Journal*, Vol. 28, No. 6, 1990, pp. 995–1004.

[17] Lambourne, N. C., and Bryer, D. W., "The Bursting of Leading-Edge Vortices—Some Observations and Discussion of the Phenomenon," Aeronautical Research Council, R&M 3282, April 1961.

[18] Ericsson, L. E., "Vortex Breakdown Dynamics on Pitching Delta Wings," AIAA Paper 95-1777, June 1995.

[19] Huang, X. Z., and Hanff, E. S., "Roll Rate Induced Camber Effect on Delta Wing Leading-Edge Vortex Breakdown," AIAA Paper 95-1793, June 1995.

[20] Ericsson, L. E., and Hanff, E. S., "Further Analysis of High-Rate Rolling Experiments of a 65 Deg Delta Wing," *Journal of Aircraft*, Vol. 31, No. 6, 1994, pp. 1310–1317.

[21] Ericsson, L. E., and Beyers, M. E., "Nonlinear Rate and Amplitude Effects on AGARD WG16 Generic Combat Aircraft Model," AIAA Paper 98-0409, Jan. 1998.

[22] Bergmann, B., Hummel, D., and Oelker, H.-C., "Vortex Formulation over a Close-Coupled Canard-Wing-Body Configuration in Unsymmetrical Flow," AGARD, CP-494 July 1991 (Paper 14).

[23] Ericsson, L. E., and Beyers, M. E., "Conceptual Fluid/Motion Coupling in the Herbst Supermaneuver," *Journal of Aircraft*, Vol. 34, No. 3, 1997, pp. 271–277.